Extreme Resilience in Cochleate Nanoparticles

Tamás Bozó†, Richárd Brecska†, Pál Gróf†, and Miklós S. Z. Kellermayer*†‡

†Department of Biophysics and Radiation Biology, and ‡MTA-SE Molecular Biophysics Research Group, Semmelweis University, Tűzoltó utca 37-47, Budapest 1094, Hungary

Langmuir, 2015, 31 (2), pp 839–845

DOI: 10.1021/la504428x

Publication Date (Web): December 18, 2014

*E-mail: kellermayer.miklos@med.semmelweis-univ.hu.

Extreme resilience in cochleate nanoparticles

*Tamás Bozó[1], Richárd Brecska[1], Pál Gróf[1], Miklós S. Z. Kellermayer[1,2,]**

[1]Semmelweis University, Department of Biophysics and Radiation Biology, 1094, Budapest, Tűzoltó u. 37-47., Hungary

[2]MTA-SE Molecular Biophysics Research Group, Semmelweis University, 1094, Budapest, Tűzoltó u. 37-47., Hungary

KEYWORDS: cochleate; membrane roll; force spectroscopy; nanomechanics; atomic force microscopy; myelin sheath

ABSTRACT Cochleates, prospective nanoscale drug delivery vehicles, are rolls of negatively-charged phospholipid membrane layers. The membrane layers are held together by calcium ions; however, neither the magnitude of membrane-interaction forces, nor the overall mechanical properties of cochleates have been known. Here we manipulated individual nanoparticles with atomic force microscopy to characterize their nanomechanical behavior. Their stiffness (4.2-12.5 N/m) and membrane-rupture forces (45.3-278 nN) are orders magnitude greater than those of the tough viral nanoshells. Even though the fundamental building material of cochleates is a fluid membrane, the combination of supramolecular geometry, the cross-linking action of calcium and the tight packing of the ions apparently lead to extreme mechanical resilience. The supramolecular design of cochleates may provide efficient protection for encapsulated materials

and give clues to understanding biomolecular structures of similar design, such as the myelinated axon.

Introduction

Cochleates are membrane rolls made of dipalmitoyl phosphatidylserine and calcium ions, and are so named because of their cross-sectional geometry.[1] In a cochleate particle the spirally curving and stacked lipid layers are stabilized by calcium ions that cross-link the negatively charged lipid headgroups.[1, 2, 3] Cochleates have been proposed to be used as biocompatible pharmaceutical vehicles for molecules which are difficult to deliver such as amphotericin B to treat systemic mycoses,[2, 3, 4, 5, 6] factor VIII for replacement in haemophilia A,[7, 8] or antigens for immunization.[9, 10, 11, 12, 13, 14, 15] In certain applications the active agent itself, rather than calcium, serves as the electrostatic glue that holds the membrane sheets together.[16, 17, 18, 19, 20, 21] The structure of cochleates has previously been analyzed by using freeze fracture,[1, 3, 12, 22] negative staining,[7, 23, 24] scanning electron[12, 21, 25] and light microscopies.[3, 10, 12, 21] Although a detailed model has emerged about the geometry of cochleates, very little is known about their internal dynamics, mechanical properties and the structure-stabilizing forces. Considering that the cochleate displays a highly ordered structure in spite of being composed of a fluid membrane, its elasticity and viscosity need to be investigated experimentally. In the present work we mechanically manipulated individual cochleate nanoparticles by using atomic force microscopy and *in situ* force spectroscopy and found that they display unusually high stiffness and mechanical rupture forces.

Experimental

Materials

Dioleoyl phosphatidylserine (1,2-Dioleoyl-sn-Glycero-3-[Phospho-L-Serine], DOPS) was obtained from Avanti Polar Lipids, Inc. (Alabaster, Alabama, USA). Whatman Nuclepore membrane filters (d=100 nm, track-etched membranes), chloroform, sodium azide and 1 M calcium chloride solution were purchased from Sigma Aldrich Kft. (Budapest, Hungary). Argon 5.0 and nitrogen 5.0 gases were from Linde Gáz Magyarország Zrt. (Budapest, Hungary). Purified water was produced by a Milli-Q Integral 3 Water Production Unit (Merck Millipore, Billerica, MA, USA). Round mica sheets were obtained from Ted Pella, Inc. (Redding, CA, USA).

Methods

Preparation of cochleates

Cochleates were obtained from small unilamellar vesicles (SUV-s) prepared by the extrusion method.[26] Briefly, 500 µl 20 mg/ml DOPS/chloroform stock solution was pipetted to a clean glass tube, and the organic solvent was evaporated under Ar gas stream. The lipid film was placed in vacuum (<20 Hgmm) for 30 min. to remove organic solvent traces, then hydrated with 2 mM NaN_3 in 100 µl aliquots to 1 ml final volume during vigorous vortexing. The resultant milky suspension (lipid concentration: 10 mg/ml, 12.4 mM DOPS) was extruded 41 times through polycarbonate membrane filter with 100 nm pore diameter in an AvantiPolar Mini Extruder (Avanti Polar Lipids, Inc., Alabaster, AL, USA) at 30±0.2°C temperature. The formation of cochleates was induced by adding a calcium stock solution (12.4 mM $CaCl_2$, 2mM NaN_3) dropwise to the SUV preparation until an equimolar ratio of Ca^{2+} and DOPS was reached. The final lipid concentration was ~6.2 mM (5 mg/ml). The SUV sample turned opaque upon

Ca^{2+} addition, and visible precipitation occurred. The sample was then incubated at 25±1°C for 1 week.

AFM imaging and force spectroscopy

50 µl precipitated pellet was harvested from the cochleate sample and diluted with 200 µl purified water. 50 µl of this sample was applied to the surface of freshly cleaved mica and, after 1 minute incbation, washed gently with purified water and dried in a stream of N_2 gas of high purity. Cochleates were imaged with a Cypher instrument (Asylum Research, Santa Barbara, CA) with 0.4 to 1 Hz line-scanning rate in air. A silicon cantilever (OMCL AC-160TS, Olympus, Japan) was used in non-contact mode, oscillated at its resonance frequency (300-320 kHz, typically). Force spectra were taken in contact mode at defined locations of previously scanned areas and at constant 1 µm/s velocity. The cantilevers (stiffness typically around 35 N/m) were calibrated by the thermal method.[27] Temperature during the measurements was 29±1°C.

Image analysis

Images were analyzed by using the built-in algorithms of the AFM driving software (IgorPro, WaveMetrics Inc., Lake Oswego, OR). AFM amplitude contrast images are shown in this paper. To determine height variations, height contrast data were used.

Statistical analysis of data

For phase "b" and "d" peak number analysis (**Figure 4. b**) only four-phase curves (n= 18) were used. The selected force spectra were used for peak-to-peak analysis (**Figure 5. a**). Step size data (**Figure 5. e**) were gathered from 8 individual cochleates. For stiffness determination (**Figure 6.**

a) not only complete but partial force curves (i.e., ones containing a complete phase "a" and partial "b") were used as well (total n=40). To assemble the force-peak histogram (**Figure 6. b**), the same 18 spectra were analyzed that were used for peak number analysis. Scatter plots and histograms were created in Origin 7 software (OriginLab Ltd., Northampton, Ma, USA).

Results and Discussion

Morphology of cochleates

Atomic force microscopy of surface-adsorbed cochleate nanoparticles revealed a roll-like topographical appearance with varying axial and cross-sectional dimensions (**Figure 1. a** and **b**). Their overall structural features appeared consistent with the model suggested previously based on freeze-fracture electron microscopy observations.[1] The diameter of the rolls usually varied gradually along the longitudinal axis because the edge of the underlying lipid sheets extended to different distances (see **Figures 1, 2. c** and **5.b**). Liposome aggregates often associated with the cochleates (see **Figures 1. a**, **c**, **2. c** and **5. b**). Certain rolls flattened on the surface (**Figure 1. c**) at one end with the other end remaining cylindrical. Such a capacity for flattening points at the presence of cavity inside the roll. While cochleates are usually thought of as compact structures with no internal aqueous space,[28] our observations indicate that under some circumstances a hollow core may be present. This observation supports recent electron microscopy findings.[29] Occasionally, ribbed cochleates were observed (**Figure 1. d**) which resembles multilamellar protein-bearing cochleates seen earlier with freeze fracture electron microscopy.[12] The topographical appearance suggests that axial compressive forces may have led to the formation of riblike surface ridges.

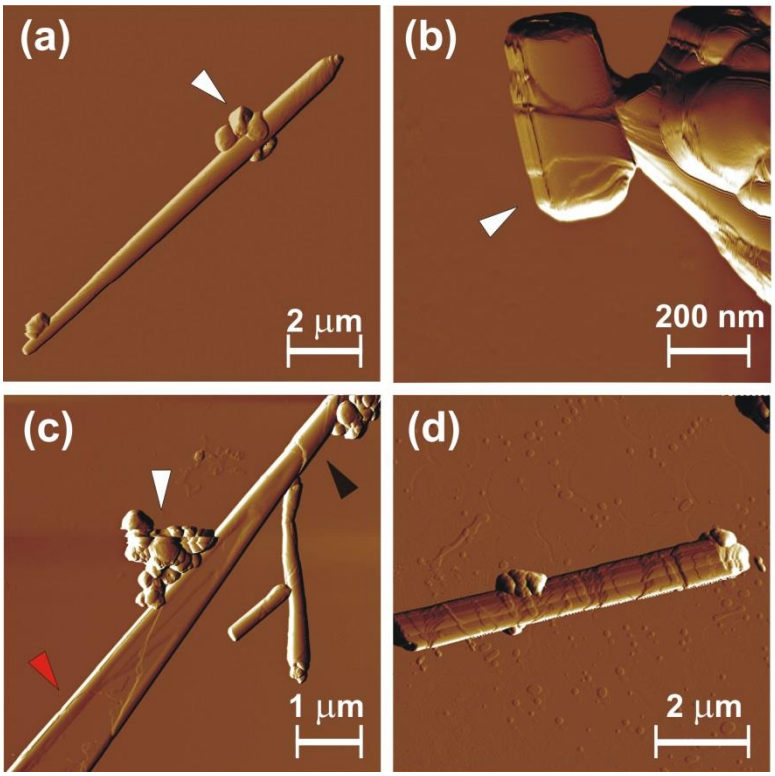

Figure 1. Morphology of cochleates. (a) Needle-like lipid roll associated with a few liposomal particles attached (white arrowhead). (b) Cochleate particle (white arrowhead) displaying topographical steps corresponding to superimposed and staggered lipid layers. (c) Cochleate flattened at one end (red arrowhead) and compacted at the other (black arrowhead). White arrowhead points at liposomal aggregate. (d) Cochleate with surface ridges.

Force spectroscopy

Reversible deformation of cochleates

We mechanically manipulated individual cochleate nanoparticles by pressing the AFM tip into their surface at specific locations then pulling the cantilever back at a constant velocity (**Figure 2. a**). When cochleates were loaded with forces up to 50 nN, no hysteresis was seen between the approach and retraction data (for typical force curves, see **Figure 2. b)** indicating that the

deformation was reversible on the time scale of a single mechanical cycle (~10 ms). To check for reversibility on a longer (minute) time scale, we loaded cochleates in 100 successive mechanical cycles at the same location. Neither changes in the slope of the force curves, nor the appearance of transitions were apparent (**Figure 2. b** inset). Furthermore, no permanent depressions on the cochleate surface were observable as a result of the manipulation (**Figure 2. c**). Thus, cochleates are resilient structures able to bear successively applied high forces without material fatigue or irreversible deformation.

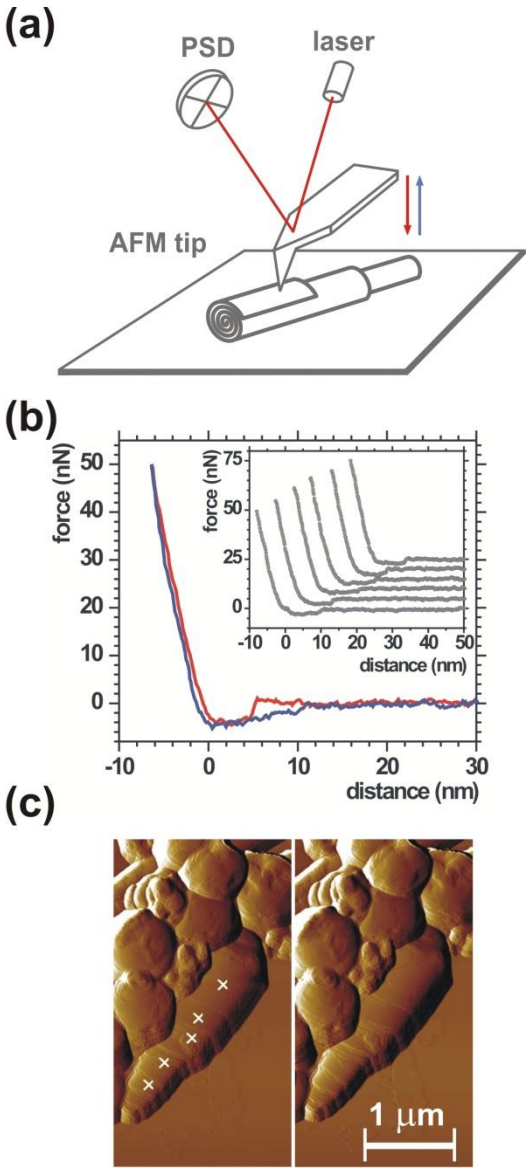

Figure 2. (a) Schematics of the force spectroscopy experiment. Force was obtained from the bending of a calibrated cantilever as a function of the distance traveled towards the substrate surface (PSD: position sensitive diode). (b) Approach (red) and retraction (blue) force curves collected at a maximum 50 nN loading force. Inset shows the first, 20th, 40th, 60th, 80th and 100th approach curves (gradually shifted for better display) of a 100-curve mechanomanipulation series taken from the same location. (c) Cochleate prior to (left image) and following (right image) force spectroscopy. 100 cycles at max. 50 nN force were carried out at each point marked with white crosses.

Unique nanomechanical fingerprint revealed by pressing with excessive forces

Upon increasing the maximum load above a critical value, irreversible transitions became apparent in the force spectra, and a large hysteresis occurred between the approach and retraction traces. A typical force curve is shown in **Figure 3. a**.

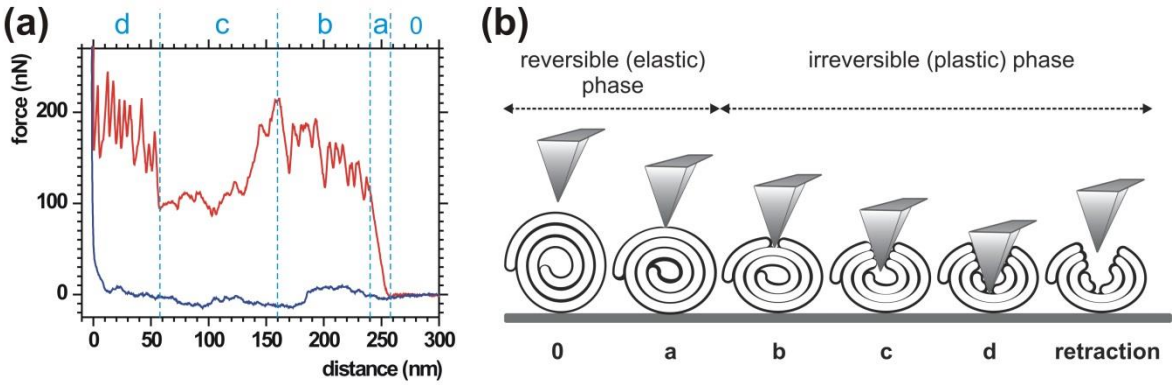

Figure 3. (a) Representative force spectrum. Red and blue lines correspond to data collected during cantilever approach and retraction, respectively. Distance in nm denotes the position of

the cantilever tip relative to the mica surface. (b) Model of cochleate mechanomanipulation. Letters below the diagram correspond to phases shown in (a).

The approach curve could be divided into four distinct phases. After a featureless, constant-force region that corresponds to the unloaded movement of the cantilever towards the cochleate surface (indicated by “0”) a steep force rise emerged (phase “a”) that turned into a series of sawtooth-like peaks (phase “b”). This period ended with a transient force drop and an unstructured region (phase “c”) that transformed into another series of sawtooth force peaks (phase “d”) before force abruptly increased. Retraction curves were featureless on the force-scale of the approach, suggesting that in this phase there was no significant mechanical load on the cantilever. The well-structured and highly reproducible shape of the force spectra reflects a complex fingerprint that carries information about both the construction and the nanomechanical properties of the cochleate. In region “0” there is no contact between the tip and the sample, therefore the force is zero (see graphical interpretation of phases in **Figure 3. b**). Upon contact, the tip applies pressure on the membrane roll, therefore the cantilever bends and force rises steeply (phase “a”). Linearity of this region implies that the cochleate displays Hookean elasticity. The ideally elastic behavior is also substantiated by reversibility in this regime (see **Figure 2.**). Successive peaks of phase “b” likely correspond to the rupture of individual phospholipid bilayers. Once the tip reaches the hollow core of the membrane roll, resistance drops, hence force decreases and the curve becomes devoid of distinct features (phase “c”). Upon pushing the cantilever tip further, force begins to increase and successive peaks re-appear (phase “d”), implying that the membrane layers in the bottom half of the cochleate are reached and are broken through. Finally, the abrupt force increase at the end of phase "d" is likely caused by the cantilever tip reaching the mica surface, suggesting that the cochleate was, in this experiment,

pierced through its entire diameter. In some cases, phase “c” was absent and phases “a” and “d” merged, which may be explained by the lack of hollow core.

To validate the molecular events underlying the consensus force spectrum, we carried out detailed analyses of its features and compared them with topographical data.

To test whether during nanomanipulation the cochleate was pierced through its full diameter, we compared the contact height (sum of phases "a" through "d" in **Figure 3.**) with the topographical height at the site of the manipulation obtained from AFM images. We found a very close correlation between these parameters (**Figure 4. a**), indicating that the force spectrum indeed reflects the events associated with a cantilever tip breaking through the entire stack of membrane layers within the cochleate nanoparticle. This conclusion furthermore predicts that phases "b" and "d" display similar number of force peaks, because the top and bottom halves of the cochleate are expected to contain similar numbers of membrane layers. In support, we found a good correlation between the numbers of phase "b" and "d" force peaks (**Figure 4. b**). Deviation from a closer correlation may be caused by missing force peaks due to sudden, simultaneous rupture of more than one superpositioned membrane layer, in any half of the cochleate.

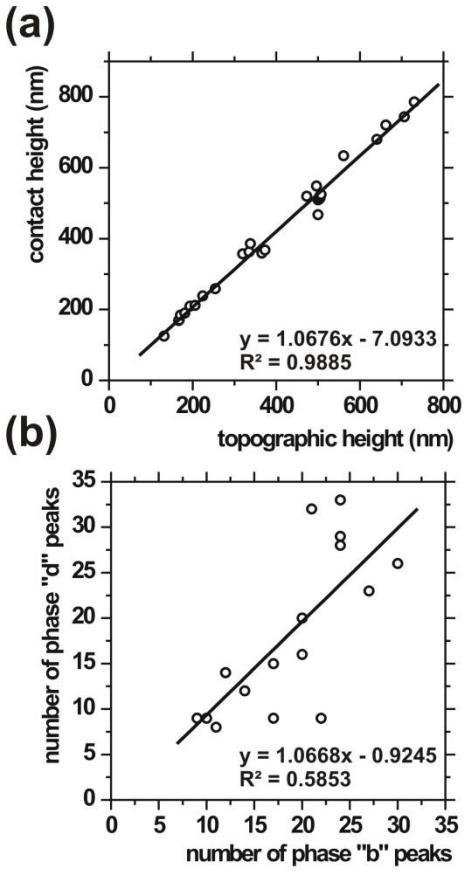

Figure 4. Correlation between (a) contact and topographic heights of cochleates (n=29) and (b) the number of peaks in phases „b" and „d" of the force curves (n=18).

To test whether phase "b" and "d" force peaks correspond to membrane layer breakthrough transitions, we measured the distribution of distance gain between consecutive peaks (**Figure 5. a**). The peak-to-peak distance histograms of both "b" and "d" phases display an apparently multimodal distribution (**Figure 5. a**). The highest peak is at approximately 5 nm which corresponds well to the thickness of a single phospholipid bilayer.[30, 31] Accordingly, most of the transitions manifested in a force sawtooth correspond to events during which a single bilayer was mechanically broken through. Interestingly, further maxima appeared at integer multiples of ~2.5

nm, suggesting that monolayers or layer combinations can also be broken through in a single transition. This finding supports our intepretation of the deviation from perfect correlation in the peak number analysis (**Figure 4. b**). If the histogram peaks correspond to the distance gain caused by breaking through the lipid layer components of the cochleate, then a similar topographical step height distribution may be observed on the surface of the nanoparticle. We tested this hypothesis by a detailed surface topography analysis (**Figures 5. b-d**). The step height distribution showed a major peak between 5 and 6 (**Figure 5. e**), which is in excellent agreement with the distribution of peak-to-peak distances implying that it is indeed monolayers and bilayer combinations that are broken through during mechanomanipulation of cochleates. Altogether, the mechanical fingerprint (**Figure 3. a**) displays the elastic and plastic deformations of the cochleate nanoparticle. The plastic deformation is thus caused by the sequential rupture of the component lipid membrane sheets in integer multiples of a monolayer.

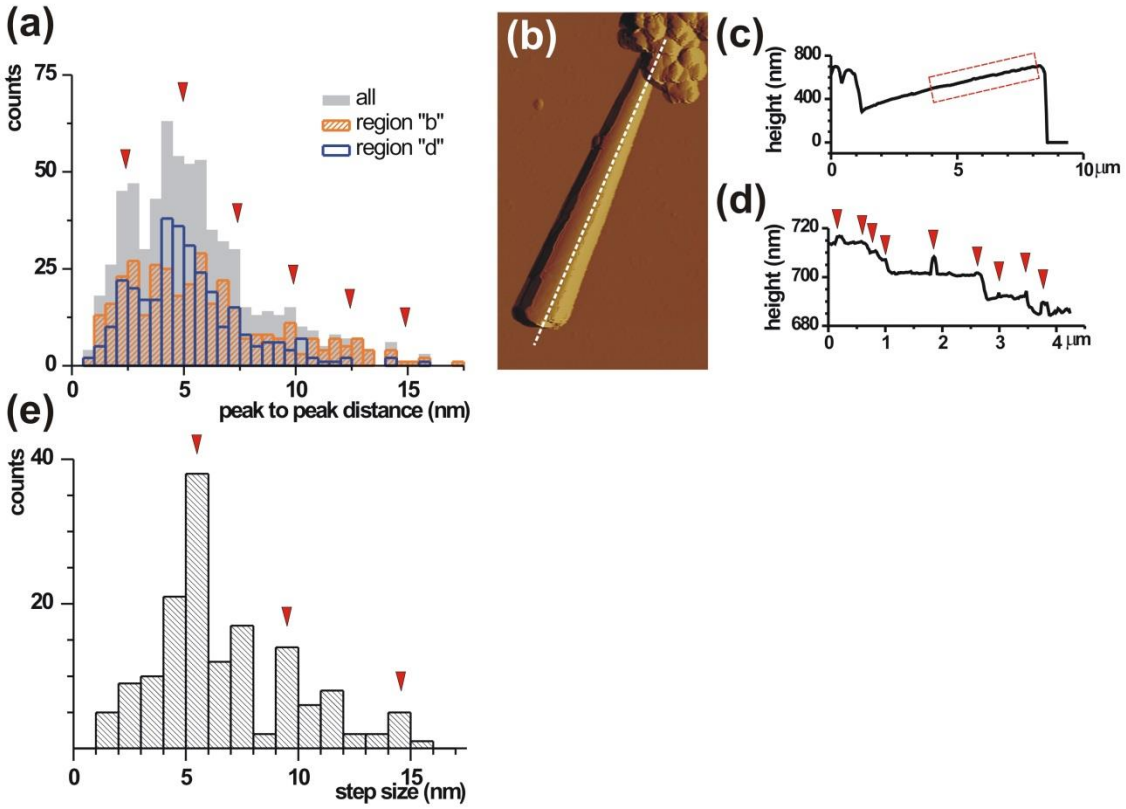

Figure 5. (a) Distribution of peak-to-peak distances in the different regions of the force curves (n_b=356 , n_d=313). Red arrowheads point at histogram modes. (b) Amplitude-contrast image of a cochleate. The white dashed line shows the section along which a detailed topographical analysis was carried out (c-d). (c) Topographical height distribution along the cochleate nanoparticle in (b). Framed region is magnified further in (d). (d) Topographical height profile along the cochleate axis corrected for overall baseline slope. Red arrowheads point at height steps. (e) Histogram of topographical step sizes with modes marked with red arrowheads (n=166).

Stiffness and mechanical resistance

The magnitude of forces necessary for either the elastic or plastic deformation reflects the mechanical properties of the cochleate and is related to the stability of the nanoparticle. The slope of the force curve's linear region (phase "a") corresponds to the stiffness (spring constant) of the membrane structure according to Hooke's law of elasticity.[32] The spring constant of cochleates is surprisingly large (8.2±1.5 N/m, see **Figure 6. a**), orders of magnitude greater than that of empty viral capsids, liposomes, supported lipid bilayers or microtubules (**Table 1.**). Considering that the lipid bilayer displays fluidlike behavior, the observation of such an extreme stiffness is unexpected.

Table 1. Mechanical properties of ordered nanoscale biomolecular systems

	Spring constant (N/m)	Rupture force (nN)	References
Empty viral capsids	0.11 - 1.03	0.6 - 5.8	33, 34, 35, 36, 37
Liposomes	0.01 - 0.12	0.6 - 1.1	38, 39
Supported lipid bilayers	0.01 - 1	0.4 - 36	40, 41, 42
Microtubules	0.074 - 0.1	0.3 - 0.5	43, 44

Furthermore, cochleate membrane layers could withstand forces up to a few hundred nN prior to rupture (**Figure 6. b**). By comparison, the force needed to rupture a covalent bond is a few nN (1.4±0.3 nN for S-Au and 2.0±0.3 nN for Si-C bonds, respectively).[45] Highly ordered protein structures, such as microtubules or viral capsids suffer failure upon exposure to a few hundred pN to few nN forces. Even planar lipid bilayers supported by hard substrate break through at forces below a few tens of nN depending on the type of AFM tip, lipid composition, temperature and buffer conditions (see **Table 1.**). Calcium may increase the mechanical resistance of phospholipid bilayers[46] and it has a pronounced effect on negatively charged lipids.[40, 47] However, the lipid headgroup ordering effect of calcium ions cannot solely account for the anomalously tough mechanical properties of cochleates. Most plausibly a combination of the

onion-shell geometry, the local cross-linking of lipid headgroups between neighboring membrane sheets by calcium ions and the parallel coupling of these interactions along the plane of the membrane leads to the extreme mechanical stability and stiffness. Because of the parallel coupling of calcium-based cross-links between neighboring lipid bilayers, a high shear force is required for the displacement of a membrane on top of an underlying one (**Figure 7. a**). In a nanomechanical experimental setting this shear force is the tangent-vector component of the deforming force (**Figure 7. b**), explaining why high forces are required for both elastic and plastic deformations. Furthermore, we hypothesize that the tight packing of calcium ions between the bilayers places a strong constraint on lateral diffusion so much that a quasi-crystalline phase is formed. During plastic deformation the membrane sheets are shifted by the high deforming forces, but because of the quasi-crystalline structure restoring forces do not arise. Thus, the deformation is expected to persist.

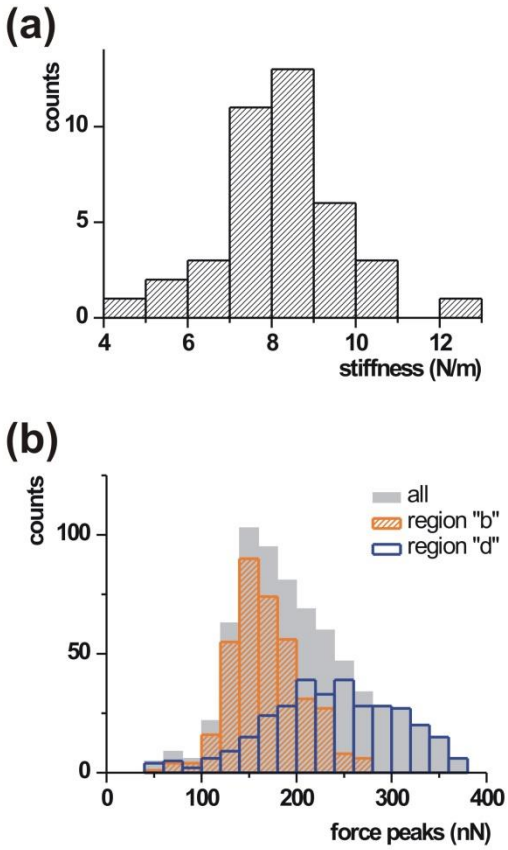

Figure 6. (a) Histogram of cochleate stiffness (n=40). (b) Histogram of peak forces (n_b=373 and n_d=330) .

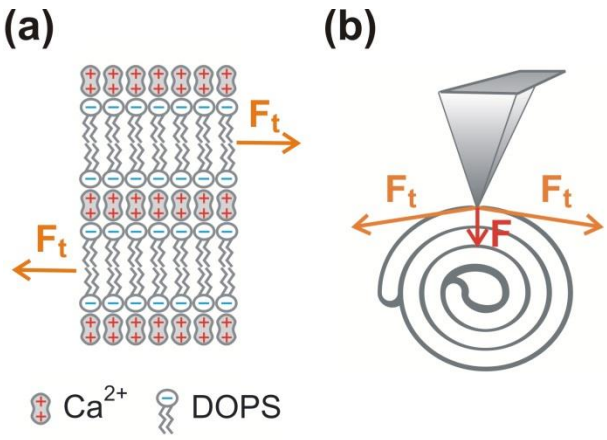

Figure 7. (a) Schematics of the cross-sectional structure of cochleate membrane layers. $\boldsymbol{F_t}$ corresponds to the shear force necessary for membrane-sheet displacement. (b) Schematics of AFM mechanomanipulation illustrating the tangential components of the deforming force.

Plastic deformation of cochleates

To test the prediction of irreversible plastic deformation, we exposed a cochleate nanoparticle to repeated cycles of loading with excessive forces (**Figure 8.**). We found that only the first mechanical cycle displayed the characteristic mechanical fingerprint, and the subsequent cycles were essentially devoid of transitions and hysteresis (**Figure 8. a**). Furthermore, the plastic deformation resulted in a permanent depression in the cochleate surface that could be detected by AFM imaging (**Figures 8. b-c**).

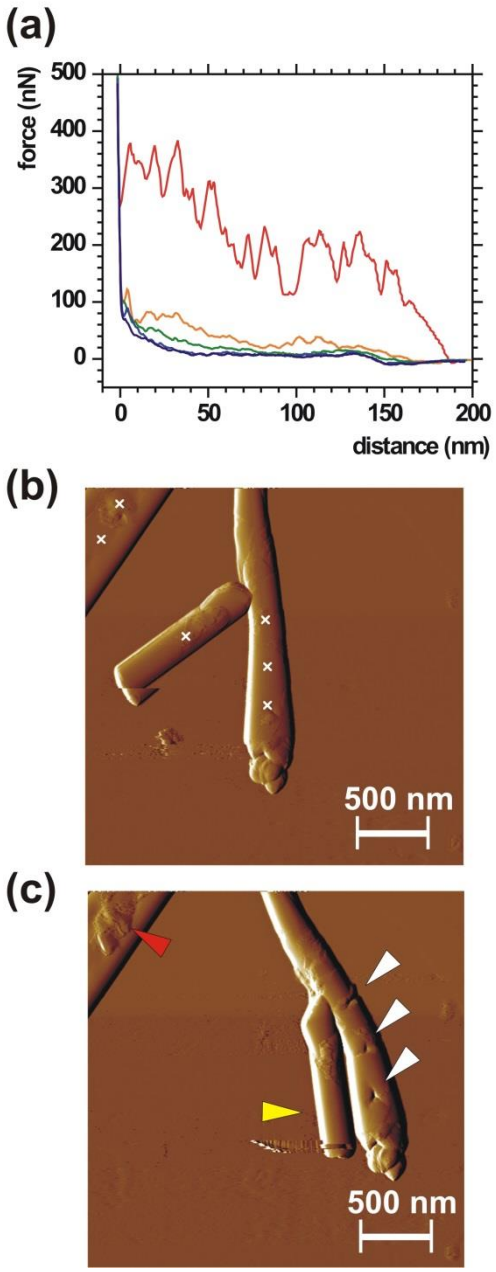

Figure 8. Plastic deformation of cochleates. (a) Successive approach curves from the first (red) to the fifth (violet) in temporal order. Cochleates prior to (b) and following (c) force spectroscopy at the points marked with white crosses. Structural rearrangements due to mechanomanipulation are marked with colored arrowheads. Red arrowhead points at a site where membrane sheets bulged out of the cochleate surface. White arrowheads point at surface

depressions. Yellow arrowhead points at a cochleate which was repositioned on mica as a result of the nanomechanical manipulation.

Conclusions

In summary, AFM imaging and force spectroscopy uncovered both the topological features and surface-hidden structural details of phospholipid membrane rolls. Cochleates not only withstand forces up to 100 nN without rupture, but within this force range they display ideal elasticity. Upon exposure to forces well exceeding 100 nN, a characteristic nanomechanical fingerprint emerges with transitions corresponding to the sequential breaking through lipid layers. Because of calcium-dependent coupling within the onion-shell-like cross-sectional structure of the cochleate, a quasi-crystalline order is maintained the mechanical distorsion of which results in plastic deformation upon exposure to extreme forces. The results presented in this work were obtained on partially hydrated cochleates under ambient humidity conditions, and their properties in fully submerged aqueous conditions are yet to be characterized. However, cochleates have emerged here as resilient nanoparticles with extreme mechanical properties far exceeding those of tough viral nanoshells and complex molecular architectures designed for mechanical resistance. Thus, the geometry and the internal interactions of cochleates may make them ideal for mechanical protection. Although in myelinated sheaths protein molecules rather than calcium ions stabilize the underlying membrane sheets, because of their structural similarity to cochleates the myelinated sheath may, intriguingly, also function as a mechanical barrier for the enveloped neuronal axon. In a technological setting cochleates, as pharmaceutical vehicles, may provide unparalleled protection for the molecular species to be carried harmlessly towards its destination.

Supporting Information. Supporting Information Available: Cochleate internal cavity analysis; Force curves. This material is available free of charge via the Internet at http://pubs.acs.org.

AUTHOR INFORMATION

Corresponding Author

E-mail: kellermayer.miklos@med.semmelweis-univ.hu

Author Contributions

The manuscript was written through contributions of all authors. All authors have given approval to the final version of the manuscript.

Notes

The authors declare no competing financial interest.

ACKNOWLEDGMENT

This work was supported by grants from the Hungarian Science Foundation (OTKA K84133, OTKA K109480). The research leading to these results has received funding from the European Union's Seventh Framework Program (FP7/2007-2013) under grant agreement n° HEALTH-F2-2011-278850 (INMiND).

ABBREVIATIONS

AFM, atomic force microscope; DOPS, dioleoyl phosphatidylserine; PSD, position sensitive diode; SUV, small, unilamellar vesicle.

REFERENCES

1. Papahadjopoulos, D.;Vail, W. J.;Jacobson, K.; Poste, G. Cochleate lipid cylinders: formation by fusion of unilamellar lipid vesicles. *Biochim. Biophys. Acta* **1975**, *394*, 483-491.

2. Zarif, L.;Graybill, J. R.;Perlin, D.; Mannino, R. J. Cochleates: New lipid-based drug delivery system. *J. Liposome Res.* **2000**, *10*, 523-538.

3. Zarif, L.; Graybill, J. R.; Perlin, D.; Najvar, L.; Bocanegra, R.; Mannino, R. J. Antifungal activity of amphotericin B cochleates against Candida albicans infection in a mouse model. *Antimicrob. Agents Chemother.* **2000**, *44*, 1463-1469.

4. Santangelo, R.; Paderu, P.; Delmas, G.; Chen, Z. W.; Mannino, R.; Zarif, L.; Perlin, D. S. Efficacy of oral cochleate-amphotericin B in a mouse model of systemic candidiasis. *Antimicrob. Agents Chemother.* **2000**, *44*, 2356-2360.

5. Segarra, I.; Movshin, D. A.; Zarif, L. Pharmacokinetics and tissue distribution after intravenous administration of a single dose of amphotericin B cochleates, a new lipid-based delivery system. *J. Pharm. Sci.* **2002**, *91*, 1827-1837.

6. Delmas, G.; Park, S.; Chen, Z. W.; Tan, F.; Kashiwazaki, R.; Zarif, L.; Perlin, D. S. Efficacy of orally delivered cochleates containing amphotericin B in a murine model of aspergillosis. *Antimicrob. Agents Chemother.* **2002**, *46*, 2704-2707.

7. Miclea, R. D.; Varma, P. R.; Peng, A.; Balu-Iyer, S. V. Development and characterization of lipidic cochleate containing recombinant factor VIII. *Biochim. Biophys. Acta* **2007**, *1768*, 2890-2898.

8. Kosloski, M. P.; Peng, A.; Varma, P. R.; Fathallah, A. M.; Miclea, R. D.; Mager, D. E.; Balu-iyer, S. V. Immunogenicity and pharmacokinetic studies of recombinant factor VIII containing lipid cochleates. *Drug Deliv.* **2011**, *18*, 246-254.

9. Perez, O.; Bracho, G.; Lastre, M.; Mora, N.; del Campo, J.; Gil, D.; Zayas, C.; Acevedo, R.; Gonzalez, D.; Lopez, J. A.; Taboada, C.; Turtle, C.; Solis, R. L. Novel adjuvant based on a proteoliposome-derived cochleate structure containing native lipopolysaccharide as a pathogen-associated molecular pattern. *Immunol. Cell Biol.* **2004**, *82*, 603-610.

10. Acevedo, R.; Callico, A.; del Campo, J.; Gonzalez, E.; Cedre, B.; Gonzalez, L.; Romeu, B.; Zayas, C.; Lastre, M.; Fernandez, S.; Oliva, R.; Garcia, L.; Perez, J. L.; Perez, O. Intranasal administration of proteoliposome-derived cochleates from Vibrio cholerae O1 induce mucosal and systemic immune responses in mice. *Methods* **2009**, *49*, 309-315.

11. Del Campo, J.; Lindqvist, M.; Cuello, M.; Backstrom, M.; Cabrerra, O.; Persson, J.; Perez, O.; Harandi, A. M. Intranasal immunization with a proteoliposome-derived cochleate containing recombinant gD protein confers protective immunity against genital herpes in mice. *Vaccine* **2010**, *28*, 1193-1200.

12. Acevedo, R.; Perez, O.; Zayas, C.; Perez, J. L.; Callico, A.; Cedre, B.; Garcia, L.; McKee, D.; Mullen, A. B.; Ferro, V. A. Cochleates derived from Vibrio cholerae O1 proteoliposomes: the impact of structure transformation on mucosal immunisation. *Plos One* **2012**, *7*, e46461.

13. Infante-Bourzac, J. F.; Sifontes-Rodriguez, S.; Arencibia-Arrebola, D. F.; Hernandez-Salazar, T.; Farinas-Medina, M.; Perez, O. Toxicological Assessment of the Cochleate Derived

from Neisseria meningitidis Proteoliposome in Sprague Dawley Rats. *N. Am. J. Med. Sci.* **2012**, *4*, 135-140.

14. Perez, O.; Romeu, B.; Cabrera, O.; Gonzalez, E.; Batista-Duharte, A.; Labrada, A.; Perez, R.; Reyes, L. M.; Ramirez, W.; Sifontes, S.; Fernandez, N.; Lastre, M. Adjuvants are Key Factors for the Development of Future Vaccines: Lessons from the Finlay Adjuvant Platform. *Front. Immunol.* **2013**, *4*, 407.

15. Gould-Fogerite, S.; Kheiri, M. T.; Zhang, F.; Wang, Z.; Scolpino, A. J.; Feketeova, E.; Canki, M.; Mannino, R. J. Targeting immune response induction with cochleate and liposome-based vaccines. *Adv. Drug Deliver. Rev.* **1998**, *32*, 273-287.

16. Livne, L.; Epand, R. F.; Papahadjopoulos-Sternberg, B.; Epand, R. M.; Mor, A. OAK-based cochleates as a novel approach to overcome multidrug resistance in bacteria. *FASEB J.* **2010**, *24*, 5092-5101.

17. Sarig, H.; Ohana, D.; Epand, R. F.; Mor, A.; Epand, R. M. Functional studies of cochleate assemblies of an oligo-acyl-lysyl with lipid mixtures for combating bacterial multidrug resistance. *FASEB J.* **2011**, *25*, 3336-3343.

18. Epand, R. F.; Mor, A.; Epand, R. M. Lipid complexes with cationic peptides and OAKs; their role in antimicrobial action and in the delivery of antimicrobial agents. *Cell. Mol. Life Sci.* **2011**, *68*, 2177-2188.

19. Epand, R. F.; Sarig, H.; Ohana, D.; Papahadjopoulos-Sternberg, B.; Mor, A.; Epand, R. M. Physical properties affecting cochleate formation and morphology using antimicrobial oligo-

acyl-lysyl peptide mimetics and mixtures mimicking the composition of bacterial membranes in the absence of divalent cations. *J. Phys. Chem. B* **2011**, *115*, 2287-2293.

20. Epand, R. F.; Sarig, H.; Ohana, D.; Papahadjopoulos-Sternberg, B.; Mor, A.; Epand, R. M. Cochleate Assemblies with Antimicrobial Oaks and Lipid Mixtures in Absence of Divalent Cations: Biophysical Properties and Strategies to Overcome Drug Resistance. *Biophys. J.* **2011**, *100*, 487-487.

21. Syed, U. M.; Woo, A. F.; Plakogiannis, F.; Jin, T.; Zhu, H. Cochleates bridged by drug molecules. *Int. J. Pharm.* **2008**, *363*, 118-125.

22. Evans, E.; Heinrich, V.; Ludwig, F.; Rawicz, W. Dynamic tension spectroscopy and strength of biomembranes. *Biophys. J.* **2003**, *85*, 2342-2350.

23. Flach, C. R.; Mendelsohn, R. A new infrared spectroscopoic marker for cochleate phases in phosphatidylserine-containing model membranes. *Biophys. J.* **1993**, *64*, 1113-1121.

24. Ramani, K.; Balasubramanian, S. V. Fluorescence properties of Laurdan in cochleate phases. *Biochim. Biophys. Acta* **2003**, *1618*, 67-78.

25. Campo, J. D.; Zayas, C.; Romeu, B.; Acevedo, R.; Gonzalez, E.; Bracho, G.; Cuello, M.; Cabrera, O.; Balboa, J.; Lastre, M. Mucosal immunization using proteoliposome and cochleate structures from Neisseria meningitidis serogroup B induce mucosal and systemic responses. *Methods* **2009**, *49*, 301-308.

26. MacDonald, R. C.; MacDonald, R. I.; Menco, B. P.; Takeshita, K.; Subbarao, N. K.; Hu, L. R. Small-volume extrusion apparatus for preparation of large, unilamellar vesicles. *Biochim. Biophys. Acta* **1991**, *1061*, 297-303.

27. Hutter, J. L.; Bechhoefer, J. Calibration of atomic-force microscope tips. *Rev. Sci. Instrum.* **1993**, *64*, 1868-1873.

28. Zarif, L. Elongated supramolecular assemblies in drug delivery. *J. Control. Release* **2002**, *81*, 7-23.

29. Nagarsekar, K.; Ashtikar, M.; Thamm, J.; Steiniger, F.; Schacher, F. H.;Fahr, A.; May, S. Electron Microscopy and Theoretical Modeling of Cochleates. *Langmuir*, in press, DOI: 10.1021/la502775b.

30. Papahadjopoulos, D.; Miller, N. Phospholipid model membranes. I. Structural characteristics of hydrated liquid crystals. *Biochim. Biophys. Acta* **1967**, *135*, 624-638.

31. Wachtel, E.; Bach, D.; Miller, I. R. Room temperature ordering of dipalmitoyl phosphatidylserine bilayers induced by short chain alcohols. *Chem. Phys. Lipids* **2013**, *175-176*, 20-26.

32. Vinckier, A.; Semenza, G. Measuring elasticity of biological materials by atomic force microscopy. *FEBS Letters* **1998**, *430*, 12-16.

33. Roos, W. H.; Gertsman, I.; May, E. R.; Brooks, C. L.; Johnson, J. E.; Wuite, G. J. L. Mechanics of bacteriophage maturation. *P. Natl. Acad. Sci. USA* **2012**, *109*, 2342-2347.

34. Snijder, J.; Reddy, V. S.; May, E. R.; Roos, W. H.; Nemerow, G. R.; Wuite, G. J. Integrin and defensin modulate the mechanical properties of adenovirus. *J. Virol.* **2013**, 87, 2756-2766.

35. Ivanovska, I.; Wuite, G.; Jonsson, B.; Evilevitch, A. Internal DNA pressure modifies stability of WT phage. *P. Natl. Acad. Sci. USA* **2007,** *104*, 9603-9608.

36. Michel, J. P.; Ivanovska, I. L.; Gibbons, M. M.; Klug, W. S.; Knobler, C. M.; Wuite, G. J.; Schmidt, C. F. Nanoindentation studies of full and empty viral capsids and the effects of capsid protein mutations on elasticity and strength. *P. Natl. Acad. Sci. USA* **2006,** *103*, 6184-6189.

37. Roos, W. H.; Radtke, K.; Kniesmeijer, E.; Geertsema, H.; Sodeik, B.; Wuite, G. J. Scaffold expulsion and genome packaging trigger stabilization of herpes simplex virus capsids. *P. Natl. Acad. Sci. USA* **2009,** *106*, 9673-9678.

38. Li, S.; Eghiaian, F.; Sieben, C.; Herrmann, A.; Schaap, I. A. Bending and puncturing the influenza lipid envelope. *Biophys. J.* **2011**, *100*, 637-645.

39. Delorme, N.; Fery, A. Direct method to study membrane rigidity of small vesicles based on atomic force microscope force spectroscopy. *Phys. Rev. E* **2006,** *74*, 030901.

40. Künneke, S.; Krüger, D.; Janshoff, A. Scrutiny of the Failure of Lipid Membranes as a Function of Headgroups, Chain Length, and Lamellarity Measured by Scanning Force Microscopy. *Biophys. J.* **2004**, *86*, 1545-1553.

41. Alessandrini, A.; Facci, P. Nanoscale mechanical properties of lipid bilayers and their relevance in biomembrane organization and function. *Micron* **2012**, 43, 1212-1223.

42. Garcia-Manyes, S.; Redondo-Morata, L.; Oncins, G.; Sanz, F. Nanomechanics of lipid bilayers: heads or tails? *J. Am. Chem. Soc.* **2010**, 132, 12874-12886.

43. de Pablo, P. J.; Schaap, I. A.; MacKintosh, F. C.; Schmidt, C. F. Deformation and collapse of microtubules on the nanometer scale. *Phys. Rev. Lett.* **2003**, *91*, 098101.

44. Schaap, I. A. T.; Carrasco, C.; de Pablo, P. J.; MacKintosh, F. C.; Schmidt, C. F. Elastic Response, Buckling, and Instability of Microtubules under Radial Indentation. *Biophys. J.* **2006**, 91, 1521-1531.

45. Grandbois, M.;Beyer, M.; Rief, M.; Clausen-Schaumann, H.; Gaub, H. E. How Strong Is a Covalent Bond? *Science* **1999**, *283*, 1727-1730.

46. Redondo-Morata, L.; Oncins, G.; Sanz, F. Force Spectroscopy Reveals the Effect of Different Ions in the Nanomechanical Behavior of Phospholipid Model Membranes: The Case of Potassium Cation. *Biophys. J.* **2012**, *102*, 66-74.

47. Pedersen, U. R.; Leidy, C.; Westh, P.; Peters, G. H. The effect of calcium on the properties of charged phospholipid bilayers. *BBA Biomembranes* **2006**, *1758*, 573-582.

Table of Contents Graphic